ELSEVIER

Journal of Power Sources 103 (2001) 42–53

JOURNAL OF POWER SOURCES

www.elsevier.com/locate/jpowsour

Charge–discharge behaviour of VRLA batteries: model calibration and application for state estimation and failure detection

A. Tenno[a,*], R. Tenno[a], T. Suntio[b]

[a]*Control Engineering Laboratory, Helsinki University of Technology, Konemiehentie 2, SF-02150 Espoo, Finland*
[b]*Power Electronics Laboratory, University of Oulu, P.O. Box 4500, SF-90401 Oulu, Finland*

Received 15 February 2001; received in revised form 8 May 2001; accepted 21 May 2001

Abstract

The dynamic behaviour of batteries can be predicted using theoretical cell model for basic processes. In this paper, this model is calibrated for two types of valve regulated lead acid (VRLA) batteries, and is applied for viewing unobservable processes in battery by observable processes. It is shown that unobservable parameters like overpotential, reaction rate, porosity, acid concentration, and other parameters of electrode can be evaluated by total current, terminal voltage and temperature of surrounding atmosphere of battery. The calibrated model is applied to distinguish between outwardly equal batteries with different backup time and cut-off time. It is shown that difference in morphology of electrodes, thickness of electrodes and quantity of electrolyte in separator are the main distinguishing parameters between batteries. These parameters can be tested online by current–voltage measurements using fast calculation method proposed in this paper.

Keywords: Battery; Lead acid; Modelling; Estimation

1. Introduction

The purpose of the paper is to propose a fast calculation method for prediction of the dynamic behaviour of valve regulated lead acid (VRLA) batteries under charging–discharging conditions. A cell model is applied for viewing electrochemical processes in battery by current–voltage measurements. The model is calibrated against experimental data, and is applied to detect initial source of differences between seemingly equal batteries.

This method is developed for analysis of backup batteries in telecommunications UPS system. The parameters of prime interest are backup time and cut-off time (i.e. time for current cut-off by value of voltage). The telecommunications UPS system is designed for nominal battery capacity and it is considered as battery failure if real backup time is lower than the nominal requirement for the UPS system.

In spite of strong attempt made in study of fast dynamic processes in battery, it was found that the charge–discharge properties and partially service lifetime cannot be predicted with single dynamic parameter like conductivity or impedance [1]. It seemed that fast dynamics of battery contain relatively little information on charge–discharge behaviour. More complex parameters based on physical model should be used to solve the monitoring and failure prediction problems of battery.

The model development history of lead acid battery starts from late 1950s. Newman and Tiedemann [2] have provided a good review of the development in the theory of flooded porous electrodes prior to 1975. The further development was made in the following lines.

1. *Cell model*. Tiedemann and Newman [3] applied flooded electrode theory to the development of a complete cell model describing the discharge behaviour of the lead acid battery system. Gu et al. [4] proposed a model for discharge, rest and charge. Nguyen et al. [5] applied similar model to VRLA batteries. They introduced state of charge (SOC) as a dynamic parameter in the model.
2. *Two-dimensional model*. Dimpault-Darcy et al. [6] proposed a 2D model. Bernardi and Gu [7] made further development. The model proposed by Gu et al. [8] is the most complete: acid stratification due to convection is accounted for in that model. The Navier–Stokes equation with Darcy's law is used for description of the fluid dynamics in porous media. The concentration profiles and flow velocities are compared with measured data.

* Corresponding author.
E-mail address: ander.tenno@hut.fi (A. Tenno).

0378-7753/01/$ – see front matter
PII: S0378-7753(01)00830-8

Nomenclature

A	active surface area per unit volume of porous electrode (cm^2/cm^3)
c	acid concentration (mol/cm^3)
c_{ref}	reference (initial) concentration
D	diffusion constant for electrolyte (mol/cm^3)
D^{eff}	diffusion in porous media
F	Faraday's constant, $F = 96{,}487$ C/mol
i_l	current density in electrolyte (A/cm^2)
i_s	current density in solid matrix of electrode (A/cm^2)
$i_{0.ref}$	exchange current density (A/cm^2)
i_{app}	applied current (A/cm^2)
j	volumetric reaction rate, i.e. current transfer density from electrolyte to solid matrix (A/cm^3)
K_1	equivalent volume to charge constant (cm^3/A s)
K_4	equivalent molarity to charge constant (mol/A s)
M	molecular weight of species (g/mol)
Q_{max}	theoretical capacity (C/cm^3)
R	universal gas constant, $R = 8.3145$ J/mol K
t_+^0	transference number, share of total current carried by H^+ ions
T	temperature (K)
U	thermodynamic equilibrium potential (V)
V_e	partial molar volume of water in electrolyte (cm^3/mol)
V_o	partial molar volume of acid in electrolyte (cm^3/mol)

Greek letters

α_a	anodic apparent transfer coefficient
α_c	cathodic apparent transfer coefficient
α_{Ah}	charging efficiency
β	tortuosity exponent
ε	porosity, volume fraction filled with acid
ϕ^l	electrolyte potential (V)
ϕ^s	solid matrix potential (V)
η	surface overpotential
κ	acid conductivity
κ^{eff}	conductivity in porous media
θ	state of charge (SOC)
ρ	density of species (g/cm^3)
σ	conductivity of bulk electrode material (S/cm)
σ^{eff}	conductivity of porous electrode (S/cm)

3. *Two-step reaction*. Simonsson et al. [9], Ekdunge and Simonsson [10], found that the dissolution process (charge transfer) is the rate-limiting step at higher overvoltage. The diffusion is rate-limiting at lower overvoltage. They proposed a new electrode reaction model. SOC was accounted for in their model. Landfors et al. [11] applied this model in cell prediction and demonstrated a good fit of model against experimental data. The porosity and acid concentration distribution in cell were measured and predicted by the model.
4. *Overcharging*. The latest progress has been made in description of the behaviour of battery under float charging. Overcharging of VRLA batteries has been analysed by Berndt et al. [12], and Berndt [13] using lumped parameter model. Their model was thoroughly tested on experimental data. The gas formation processes during recombination were analysed by Bernardi and Carpenter [14] with a distributed parameter model and Huang and Nguyen [15] with a 2D model. Newman and Tiedemann [16] demonstrated that the transport-limited electrode reaction model, proposed earlier by Simonsson et al. [9], could essentially improve the accuracy of the model.

Contribution made by this paper:

1. The cell model is modified slightly. A new function is introduced for description of the active surface area. Different morphology of porous electrode is considered functionally and in terms of essentially smaller values for tortuosity exponent.
2. The model is calibrated experimentally for eight VRLA batteries of two types.
3. The calibrated model is applied in failure detection to distinguish between seemingly equal batteries but with different backup time and cut-off time.
4. A relatively simple calculation model is proposed for online estimation of the unobservable processes in battery by float voltage and applied current measurements. The following unobservable processes can be estimated online: current density, potential, porosity and acid concentration. The volumetric reaction rate and SOC can be calculated by these parameters, as well as backup time and cut-off time of battery.
5. A fast calculation algorithm is proposed. It is possible to perform real-time simulation of charge–discharge processes. The speed of calculation is about 100 times faster than physical process (e.g. distribution of state processes in 18 layers can be evaluated with a PC with Pentium III 533 MHz processor 100+ times faster than the physical process).
6. It is shown that much faster lumped parameter model can be used for evaluation of batteries if discharge current is low ($C/I > 2$–5 h). This is a typical situation for telecommunications UPS system.

2. Model

A basic model developed for lead acid cell by White, Newman, and other authors is considered in this section. It is solved numerically, calibrated and tested on experimental

data in Section 5. The calibrated model is applied for evaluation of the state and backup time of batteries in Sections 7 and 8.

The charge–discharge behaviour of a battery depends on electrode kinetics, which in turn is affected by variation of the electrode potential in solid matrix and electrolyte, variation of the electrode porosity, and variation of the acid density in the pores of electrode.

2.1. Electrode kinetics

The electrode reaction current is related with material of electrode as follows:

$$\frac{\partial i_1}{\partial x} = Aj \tag{1}$$

where i_1 is the current density in the liquid phase in pores of electrode (A/cm^2), A the active surface area per unit volume of porous electrode (cm^2/cm^3), j the transfer current density from electrolyte to solid matrix (A/cm^2) and Aj the volumetric reaction rate (A/cm^3).

2.1.1. Surface area

The active surface area between solid and liquid phases depends on the utilisation of electrode. Constant surface area can be expected partially, if small variation of battery capacity is considered. In general, for full cycle of charging–discharging processes, the following model for surface area has been proposed in literature

$$\begin{aligned} A &= A_{\max}\theta^{\beta 1} - \text{discharge} \\ A &= A_{\max}(1-\theta^{\beta 1}) - \text{charge} \end{aligned} \tag{2}$$

where $A_{\max}$ is the maximum active surface area (cm^2/cm^3), $\beta 1$ the tortuosity exponent and θ the SOC.

2.1.1.1. Discharging. The value for tortuosity exponent is typically 1.5 [5,7] or 0.5 [8,17]. However, it was found on test batteries presented in this paper that measured voltage cannot be explained with large values of tortuosity exponent in the conditions of deep discharge. Rapid decrease of voltage at the end of discharge can be predicted with a small value of 0.5 only. Whole discharge curve can be predicted with small values quite well. Compare the model for two values of tortuosity exponent 1.5: literature (discharge) and 0.5: tested (discharge) in Fig. 1. It seemed that morphological changes of porous electrodes are more like convex ($\beta 1 = 0.5$) than concave ($\beta 1 = 1.5$) function. A concave function is not able to describe the measured voltage in the conditions of deep discharge.

Ekdunge and Simonsson [17] first suggested a small value 0.5 for tortuosity exponent. They use it for description of experimental data. Later, Gu et al. [8] used a similar small value of 0.55 for tortuosity exponent for prediction of the measured data.

Another type of model for the deposition coverage was proposed by Gu et al. [4] and used by Dimpault-Darcy et al. [6] for description of the measured data. This model could describe measured data rather well (it was also tested on test batteries presented in this paper)

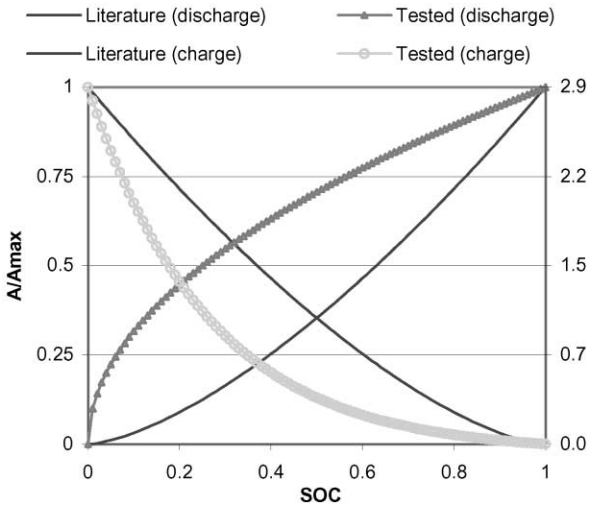

Fig. 1. Tortuosity of porous electrode: literature model and proposed model.

$$A = A_{\max}\frac{\varepsilon - \varepsilon_{\min}}{\varepsilon_{\max} - \varepsilon_{\min}} \tag{3}$$

where ε is the porosity of electrode, $\varepsilon_{\max}$ the maximum value of porosity before discharge and $\varepsilon_{\min}$ the minimum value of porosity after discharge.

The deposition coverage (Eq. (3)) terminates the discharge process rapidly, some material buried under insulating lead sulphate stays unused in the electrode. Deposition coverage can explain rapid changes of the surface area at the end of discharge in Fig. 1.

Resistance measure with direct current method is in favour of model (3). It can predict more rapid increase of resistance at the end of discharge than model (2). This was tested on test batteries. The predicted resistance used for comparison with measured data was calculated as the sum of acid resistance, charge transfer resistance and resistance of grid and connectors. The acid resistance was calculated from conductivity. The charge transfer resistance was calculated as ratio between overvoltage and applied current in entire spatial-approximation area. A constant resistance was used to take into account the grid and connectors.

However, model (3) is not practical. Estimated surface area by Eq. (3) is sensitive on minimum value of porosity. This value is not well defined. Model (2) is robust. It is more appropriate for practical use.

2.1.1.2. Charging. Recovery from deep discharge is rapid. It is much more rapid than can be predicted by power function (2) (1.5 is recommended tortuosity exponent value in literature). A good fit of model with measured data can be obtained using an exponential function (Fig. 1: tested

(charge), $\rho = 3.5$, $\gamma = 3.7$)

$$A = A_{\max}\rho\frac{\exp(-\gamma\theta) - \exp(-\gamma)}{1 - \exp(-\gamma)} \quad (4)$$

Eq. (4) is approximately equal to $A \approx A_{\max}\rho/\exp(\gamma\theta)$.

Exact morphology of porous electrode is not fully understood. Consider the description of the active surface area with empirical function (4) as experimental finding that matches well with measured data. It was found on test batteries that other models proposed in literature are less accurate than Eq. (4) regardless of values of tortuosity exponent. The following models were compared with measured data and rejected as less accurate on used sample of test batteries

$A = A_{\max}(1 - \theta^{\beta 1})$−charge [8].
$A = A_{\max}\theta^{\beta 1}(1 - \theta)^{\beta 1}$−charge–discharge [14,16].
$A = A_{\max}((\varepsilon - \varepsilon_{\min}) / (\varepsilon_{\max} - \varepsilon_{\min}))((\varepsilon_{\max} - \varepsilon)/(\varepsilon_{\max} - \varepsilon_{\min}))$−charge [4].

The approximation accuracy was also low for model with single fraction

$$A = A_{\max}\frac{\varepsilon_{\max} - \varepsilon}{\varepsilon_{\max} - \varepsilon_{\min}}$$

and for basic model (2).

Changes in morphology of porous electrode are rapid in the conditions of recovery from deep discharge and before overcharging; they are much more non-linear (Fig. 1) than can be calculated by literature models.

2.1.2. Charge

The SOC is a fraction of theoretical capacity that can be evaluated by variation of the current density from the relationship

$$\frac{\partial\theta}{\partial t} = \alpha_{\mathrm{Ah}}Q_{\max}^{-1}\frac{\partial i_1}{\partial x} \quad (5)$$

where θ is the SOC, $Q_{\max}$ the theoretical capacity (C/cm^3) and α_{Ah} the charging efficiency.

The latter parameter is defined as a ratio between required charge (Ah) and available capacity (Ah). This parameter has no meaning for discharging process. It essentially improves the model prediction accuracy of charging process. The accumulation rate of inaccuracy is 5–15% on every step if this parameter is ignored. This parameter was not used in the cell models published in literature.

2.1.3. Reaction rate

The volumetric reaction rate depends on overpotential; it is limited by acid concentration. The exchange current density and apparent transfer coefficients are specific parameters of this process

$$j = i_0\left(\frac{c}{c_{\mathrm{ref}}}\right)^{\beta 2}\left[\exp\left\{\alpha_{\mathrm{a}}\frac{F}{RT}\eta\right\} - \exp\left\{-\alpha_{\mathrm{c}}\frac{F}{RT}\eta\right\}\right] \quad (6)$$

where i_0 is the exchange current density for standard temperature of 25°C (A/cm^2), c the acid concentration (mol/cm^3), c_{ref} the reference (initial) concentration (mol/dm^3), $\beta 2$ the tortuosity exponent, η the surface overpotential, $\eta = \phi^{\mathrm{s}} - \phi^1 - U$, $\phi^{\mathrm{s}} - \phi^1$ the electrode polarisation (V), ϕ^{s} the solid matrix potential (V), ϕ^1 the electrolyte potential (V), U the thermodynamic equilibrium potential (V), α_{a} the anodic apparent transfer coefficient, α_{c} the cathodic apparent transfer coefficient, $\alpha_{\mathrm{c}} = 2 - \alpha_{\mathrm{a}}$, T the temperature (K), R the universal gas constant and F the Faraday's constant.

The exchange current density depends on temperature. The following formula can be used for correction of the exchange current density in wide temperature range [12]; it is applied in this paper

$$i_0(T) = i_0\exp\left\{\frac{E_{\mathrm{A}}(T - T_0)}{RT_0T}\right\}$$

where E_{A} is the activation energy, $E_{\mathrm{A}} = 50$ kJ/mole and T_0 the standard temperature, $T_0 = 298.2$ K (i.e. 25°C).

The thermodynamic equilibrium potential depends on acid concentration and weakly on temperature, it is equal to reference potential U_{ref} at reference concentration $c_{\mathrm{ref}} = 4.9$ mol/dm^3; in general, empirical formula $U(c, T)$ or tabulated data [13] of hydrogen electrode can be used for precise approximation, as done in this paper.

2.2. Potential in solid matrix

Ohm's law relates the current and potential in the solid matrix of electrode

$$i_{\mathrm{s}} = i_{\mathrm{app}} + \sigma^{\mathrm{eff}}\frac{\partial\phi^{\mathrm{s}}}{\partial x} \quad (7)$$

where i_{s} is the current density in solid matrix of electrode (A/cm^2), i_{app} the applied current (A/cm^2), ϕ^{s} the potential in solid matrix of electrode (V), σ^{eff} the conductivity of porous electrode, $\sigma^{\mathrm{eff}} = \sigma\varepsilon^{\beta 3}$, σ the conductivity of bulk electrode: Pb or PbO_2 (S/cm), ε the porosity of electrode, fraction of electrode saturated with acid and $\beta 3$ the tortuosity exponent.

The current conservation (charge balance requirement) is another presentation of law (7)

$$\frac{\partial i_{\mathrm{s}}}{\partial x} = \frac{\partial}{\partial x}\sigma^{\mathrm{eff}}\frac{\partial\phi^{\mathrm{s}}}{\partial x}$$

In precise analysis the solid potential can be calculated from Eq. (7) by current density.

The assumption of electroneutrality requires that charge leaving from the solid matrix must enter the pore liquid

$$i_{\mathrm{s}} - i_{\mathrm{app}} = i_1 \quad (8)$$

This is zero-divergence requirement that can be represented in the following differential form

$$\frac{\partial i_{\mathrm{s}}}{\partial x} = \frac{\partial i_1}{\partial x} \quad (9)$$

Eqs. (8) and (9) can be used for calculation of the current density in the solid matrix by current density in the liquid phase.

2.2.1. Approximation

The conductivity of the bulk electrode is high (0.5 kS/cm) for positive electrode and especially high (48 kS/cm) for negative electrode. The voltage drop is nearly zero for lead acid battery. It can be neglected in most applications without loss of accuracy.

2.3. Potential in electrolyte

Ohm's law for solution relates the current and potential in electrolyte

$$\frac{\mathrm{i}_1}{\kappa^{\mathrm{eff}}} = -\frac{\partial\phi^1}{\partial x} + \frac{RT}{F}(1-2t_+^0)\frac{\partial \ln fc}{\partial x}$$

where i_1 is the current density in electrolyte (A/cm^2), ϕ^1 the potential in electrolyte (V) and κ^{eff} the conductivity of porous electrodes and separator,

$$\kappa^{\mathrm{eff}} = \kappa\varepsilon^{\beta 4}$$

where κ is the acid conductivity (S/cm), $\kappa = \kappa_{\mathrm{ref}}$ at room temperature 25°C and acid concentration 4.9 mol/dm^3; in general, empirical formula [3] can be used for precise approximation, as done in this paper.

We have ε the porosity, volume fraction filled with acid; $\beta 4$ the tortuosity exponent; t_+^0 the transference number, share of total current carried by ions of hydrogen; f the molar activity coefficient.

This relationship in a more explicit form for molar activity can be represented as

$$\frac{i_1}{\kappa^{\mathrm{eff}}} = -\frac{\partial\phi^1}{\partial x} + \frac{RT}{F}\left[\frac{3-2t_+^0}{c} + \frac{2V_{\mathrm{o}}}{1-cV_{\mathrm{e}}}\right]\frac{\partial c}{\partial x} \tag{10}$$

where V_{o} is the partial molar volume of acid in electrolyte (cm^3/mol) and V_{e} the partial molar volume of water in electrolyte (cm^3/mol).

This formula (10) is applied for evaluation of batteries in this paper.

2.4. Electrode porosity

The porosity of electrode is a volume fraction filled with acid that can be evaluated by history of the variation of the current density from the relationship

$$\frac{\partial\varepsilon}{\partial t} = K_1\frac{\partial i_1}{\partial x} \tag{11}$$

where ε is the porosity: volume fraction filled with acid; i_1 the current density in electrolyte (A/cm^2); K_1 the equivalent volume to charge constant (cm^3/A s)

$$K_1{}^+ = \frac{1}{2F}\left(\frac{M_{\mathrm{PbSO_4}}}{\rho_{\mathrm{PbSO_4}}} - \frac{M_{\mathrm{PbO_2}}}{\rho_{\mathrm{PbO_2}}}\right), \quad \text{positive electrode}$$

$$K_1{}^- = -\frac{1}{2F}\left(\frac{M_{\mathrm{PbSO_4}}}{\rho_{\mathrm{PbSO_4}}} - \frac{M_{\mathrm{Pb}}}{\rho_{\mathrm{Pb}}}\right), \quad \text{negative electrode}$$

where M is the molecular weight of species (g/mol) and ρ the density of species (g/cm^3).

2.5. Acid concentration

The acid concentration is related with current of reaction rate and diffusion (migration) of ions as follows

$$\varepsilon\frac{\partial c}{\partial t} = \frac{\partial}{\partial x}D^{\mathrm{eff}}\frac{\partial c}{\partial x} + (cK_1 + K_4)\frac{\partial i_1}{\partial x} \tag{12}$$

where c is the acid concentration (mol/cm^3), D^{eff} the diffusion in porous media, $D^{\mathrm{eff}} = D\varepsilon^{\beta 5}$, D the diffusion constant of electrolyte (cm^2/s), ε the porosity, $\beta 5$ the tortuosity exponent, $K_4(\partial i/\partial x)$ the volumetric production rate of ions (mol/cm^3 s), K_4 the equivalent molarity to charge constant (mol/A s)

$$K_4{}^+ = \frac{2t_+^0 - 3}{2F}, \qquad K_4{}^- = -\frac{2t_+^0 - 1}{2F}$$

where t_+^0 is the transference number.

Diffusion depends on acid concentration and temperature. The diffusion constant is equal to reference value D_{ref} at standard temperature of 25°C and acid concentration of 4.9 mol/dm^3; in general, empirical formula [3] can be used for precise approximation, as done in this paper.

3. Calculation method

The battery model can be represented as the following large-scale system

$$\mathrm{d}z = [A_5 z - b(z)]\mathrm{d}t, \quad z_t = z_0 \tag{13}$$

where $z = [i_1, \phi^1, \phi^{\mathrm{s}}, \varepsilon, c, \mathrm{SOC}]^{\mathrm{T}}$-electrochemical state of battery, it contains the following processes: current density, liquid potential, solid potential, porosity, acid concentration and SOC. Every process is space-dependent, represented in L layers (L, total number of layers). The sandwich of two electrodes and separator is divided into L layers, each part of sandwich has equal number of layers; A_5, penta-diagonal matrix; b, function. It is linear, bilinear, hyperbolic or exponential, depending on the coordinate.

The model is dynamic for porosity, acid concentration and SOC. It is static for other components, i.e. current and potential ($\mathrm{d}x = 0$, $x = [i_1, \phi^1]^{\mathrm{T}}$).

The system (13) can be solved using time-iterative calculation procedure ($t = 0, \Delta t, 2\Delta t, \ldots$).

$$z_{t+1} = z_t + [A_5 z_t - b(z_t)]\Delta t, \quad z_t = z_0 \tag{14}$$

This is a two-rate system. Here current and potential are considered as dynamic processes using a small parameter technique to introduce a slow component of system.

Thickness of porous electrode is about 1 mm or less. A small sampling interval (250 ms) should be used for stable approximation of the electrode with multiple layers (Eq. (6)). Considering computational power that is available from

today's PCs, it is a great challenge to approximate electrode even with six layers.

The need for computational power can be reduced by about 100 times using sparse matrix technology [18]. The diagonal property of the matrix A_5 is used in this technology.

Using the fact that the matrix A_5 has five diagonals for acid concentration and two diagonals for all other processes, calculation procedure can be made faster still. As a result, the calculation procedure can be rendered fast enough for application in real-time simulation of charge–discharge processes. In general, it is complicated to apply 2- and 5-diagonals' properties simultaneously. However, it is simple to apply these properties if we solve system (14) for every process separately assuming that other processes are known from the last step of iteration. This separation will not produce essential inaccuracy in the case of smooth variation of process. The sampling interval is always small because of the stability requirement.

3.1. Calculation engine

The system (14) can be solved using several methods. Here are three methods. Method 1 is the simplest and fastest calculation method. Method 3 is the most accurate. The calculation efficiency and accuracy are balanced in method 2.

Method 1. Define initial state using some reference values for processes: $z = z_0$.

1. Calculate volumetric reaction rate $j(x)$ by Eq. (6) for fixed concentration and potential $z_0 = [c_0, \eta_0]$. The volumetric reaction rates in the separator and centres of electrodes are zero.
2. Solve Eq. (1) as system $A_2 i_1 = b(z_0)$ for the current density in liquid phase. Here A_2 is the double-diagonal matrix, $b(z_0)$ the power function, z_0 the SOC (fixed parameter: $z_0 = \theta_0$). The boundary condition for current density in separator is equal to applied current. It can be accounted for as follows. Change potential $\eta_0(0)$, $\eta_0(L)$ in the centres of electrodes as far as the applied current is equal to set-up value using PID-control algorithm. The boundary values for liquid potential can be calculated by this method.
3. Solve Eq. (7) as system $A_2\phi^s = b(z_0)$ for the solid potential. Here A_2 is the double-diagonal matrix, $b(z_0)$ the linear function, current density-fixed parameter: $z_0 = i_{1.0}$.

   The starting points for calculation are zero boundary values at separator surface. A back-forward solution of Eq. (7) can be used for the positive electrode and forward solution for the negative electrode. There will be free boundary values in the centre of positive and negative electrodes.
4. Solve Eq. (10) as system $A_2\phi^1 = b(z_0)$ for the liquid potential. Here A_2 is the double-diagonal matrix, $b(z_0)$ the non-linear function, current density and acid concentration-fixed parameters: $z_0 = [i_{1.0}, c_0]$.
5. Solve Eq. (11). Calculate a new value for porosity by integration in time: $\varepsilon_{t+\Delta t} = \varepsilon_t + A_2 z_0 \Delta t$. Here Δt is the step of time, A_2 the double-diagonal matrix, current density-fixed parameter: $z_0 = i_{1.0}$.
6. Solve Eq. (12). Calculate a new value for acid concentration by integration in time: $c_{t+\Delta t} = c_t + [A_5(z_0)c_t + b(z_0)]\Delta t$. Here A_5 is the penta-diagonal matrix, $b(z_0)$ the bilinear function, porosity and current density-fixed parameters: $z_0 = [\varepsilon_0, i_{1.0}]$.
7. Solve Eq. (5). Calculate a new value for SOC by integration in time: $\theta_{t+\Delta t} = \theta_t + A_2 z_0 \Delta t$. Here A_2 is the double-diagonal matrix, current density-fixed parameter: $z_0 = i_{1.0}$.

   Replace z_0 with newly calculated values and return back to step 1.

Method 2. Calculate the current density, solid and liquid potential from equation (porosity, acid concentration and SOC are fixed parameters)

$$A_2 x_t = b(x_t, y_t)$$

Calculate the porosity, acid concentration and SOC from iteration (current density, solid and liquid potential are fixed parameters)

$$y_{t+1} = y_t + [A_5 y_t - b(x_t, y_t)]\Delta t, \quad y_t = y_0$$

where $x = [i_1, \phi^s, \phi^1]^T$ is the vector of current density, solid and liquid potential; $y = [\varepsilon, c, \theta]^T$ the vector of porosity, acid concentration and SOC; A_2 the double-diagonal matrix; A_5 the penta-diagonal matrix.

Method 3. Solve two-rate system (Eq. (14)) by iteration in time. Here A_5 is the penta-diagonal matrix.

4. Battery testing

The model prediction accuracy was evaluated against measured data from the following experiment. Four batteries, connected in a string and placed into a container (Fig. 2), were charged and discharged periodically at elevated temperature of 40–48°C. A relatively low overcharging voltage 2.20 V/cell was used to prevent increased water decomposition in the experiment. The float voltage, applied current and temperature in container were measured and recorded continuously.

Two types of VRLA batteries, A and B were tested on exploitation lifetime. These batteries are similar by electrical parameters and different by design. They are produced by two different manufacturers.

Type A. Number of sections: 6. Number of positive plates: 4, negative plates: 3. Plate height: 11.3, width: 15.4 cm. Thickness of positive plate: 0.23, negative plate: 0.22 cm. Thickness of separator: 0.36 cm.

Type B. Number of sections: 6. Number of positive plates: 3, negative plates: 4. Plate height: 13, width: 11.6 cm. Thickness of positive plate: 0.32, negative plate: 0.18 cm. Thickness of separator: 0.105 cm.

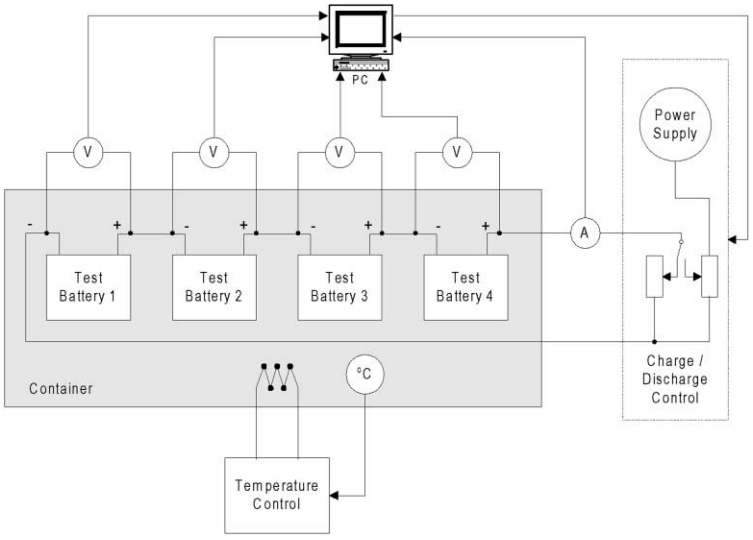

Fig. 2. Battery testing system.

5. Model calibration

Real battery build up is more complicated than what is assumed in the cell model. Thickness of porous electrode has no physical meaning for real electrode (thickness as dimension of planar electrode). However, it has meaning as an equivalent volume parameter. Thickness of porous electrodes and separator are unknown. They can be evaluated as specific parameters for battery from measured data.

Every section in battery contains six cells in parallel connection. Approximation with three cells in parallel (twice thicker electrodes) gave nearly the same calculation results, so three-cell modification was used as basic approximation model.

The applied current of model of every battery was chosen to be (as much as possible) the same as it was in the experiment (Fig. 3). A PID-controller algorithm was used to stabilise the applied current of model at measured values.

The initial values of parameters were chosen to equal parameters known from literature [4,5,13,14]. Some parameters are constant, they were not changed, other parameters were changed according to the best fit with experimental data.

The standard simplex method was used to minimise deviation of the model from the measured data. Sum of the least square errors of model was used as the criterion for minimisation.

5.1. Results

The calibrated model is shown in Tables 1–4: common parameters are in Table 1 and individual parameters for every battery are in Tables 2–4.

Thickness of porous electrode evaluated as planar electrode by battery electrical properties is about five times thinner than bulk electrode (total plate thickness). Thickness of separator is about 30% less than real separator between electrodes. It is thinner at the expense of void space filled with gases. Thickness of separator is proportional to acid volume in separator — it is equivalent volume parameter.

Rapid changes in deep discharge can be evaluated with tortuosity exponent. These changes are fast for one particular battery in both groups. They are much less rapid for other batteries. Parameters of Table 4 can be considered as a measure of morphology of electrode.

A relatively small variation between batteries was observed in charging process. The charging process parameters are more like common parameters for all test batteries (Table 5).

After calibration, a good fit of model with measured data was obtained in a wide range of charge–discharge process

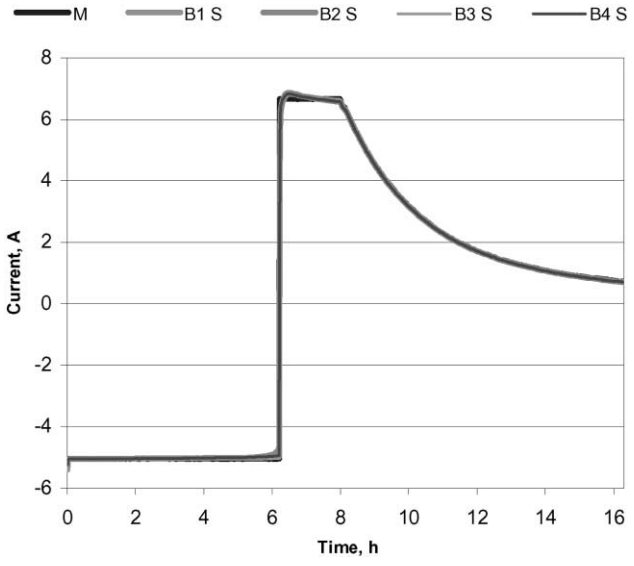

Fig. 3. Comparison of measured (M) and simulated (S) current for test batteries: B1–B4.

Table 1
Common parameters for all tested batteries

Symbol	Positive electrode	Separator	Negative electrode	Units
Q_{max}	2620	–	3120	C/cm^3
U_{ref}	1.79	–	−0.336	V
A_{max}	20.7	–	2.37	cm^2/cm^3
i_0	6.66	–	104	mA/m^2
α_a	1.15	–	1.55	–
α_{Ah}	0.9		0.9	Ah/Ah
σ	0.5		4.8	kS/cm
c_{ref}	4.9	4.9	4.9	mol/dm^3
D_{ref}	–	0.38	–	m^2/s
V_o	–	45	–	cm^3/mol
V_e	–	17.5	–	cm^3/mol
κ_{ref}	–	0.79	–	S/cm
t_+^0	–	0.72	–	–
$\beta 1$	0.85[a]	–	0.79[a]	–
$\beta 2$	1.5	–	1.47	–
$\beta 3$	0.51	–	0.51	–
$\beta 4$	1.53	1.54	1.41	–

[a] These constants are for charging process only.

(Fig. 4). The model is rather accurate in general but not everywhere, because the following processes were ignored:

- Non-faradic double-layer capacitance.
- Crystallisation effect.
- Gassing.

The model is unable to predict these processes. It takes 5 min for battery to come into steady-state condition after a long period of rest. It takes 1 min if the battery was in use lately. The model is inadequate to real process during relaxation time (1–5 min at the beginning of discharge). The relaxation time after switching from deep discharge to charge process is longer. Shorter relaxation time can be evaluated by data after [19]. This is different from our data. The gassing process has some effect in the end of charging process, causing the model to be less accurate there.

The model accuracy is rather high for most part of the charge–discharge curve (Fig. 4). On average the least square error does not differ more than 0.1 mV and maximum error more than 120 mV from measured values in the range 10.5–13.5 V. Model accuracy for charge and discharge processes is shown in Table 6.

Data on upper line is for charge and lower line for discharge. The relaxation time (5 min at the beginning of discharge and charge processes) is excluded from the error evaluation.

Table 2
Thickness of electrodes and separator (in mm) for batteries of type A

	Positive electrode	Separator	Negative electrode
Battery 1	0.590	2.256	0.403
Battery 2	0.503	2.151	0.348
Battery 3	0.555	2.259	0.385
Battery 4	0.541	2.259	0.384

6. Option for cycling analysis

The main difference between outwardly equal batteries can be seen by model. It has different values for the following parameters (Tables 2–4):

- Thickness of electrodes.
- Thickness of separator.
- Tortuosity of electrodes.

Active mass of electrodes and electrolyte volume in the test batteries evaluated by thickness of planar electrodes and separator is shown in Tables 7 and 8. Some material (up to 40–75%) is unreachable in real battery. Lead or lead dioxide

Table 3
Thickness of electrodes and separator (in mm) for batteries of type B

	Positive electrode	Separator	Negative electrode
Battery 1	0.443	2.352	0.313
Battery 2	0.601	2.438	0.441
Battery 3	0.605	2.476	0.444
Battery 4	0.599	2.394	0.440

Table 4
SOC-related tortuosity exponent in discharge reaction

Battery number type A	Positive electrode	Negative electrode	Battery number type B
1, 3, 4	0.45	0.39	2, 3, 4
2	0.26	0.22	1

Table 5
The charging process parameters

	Positive electrode, ρ	Negative electrode, ρ	Both electrodes, γ
Battery 1	3.547	3.746	3.605
Battery 2	3.501	3.074	3.496
Battery 3	3.847	3.787	3.787
Battery 4	3.565	3.735	3.749

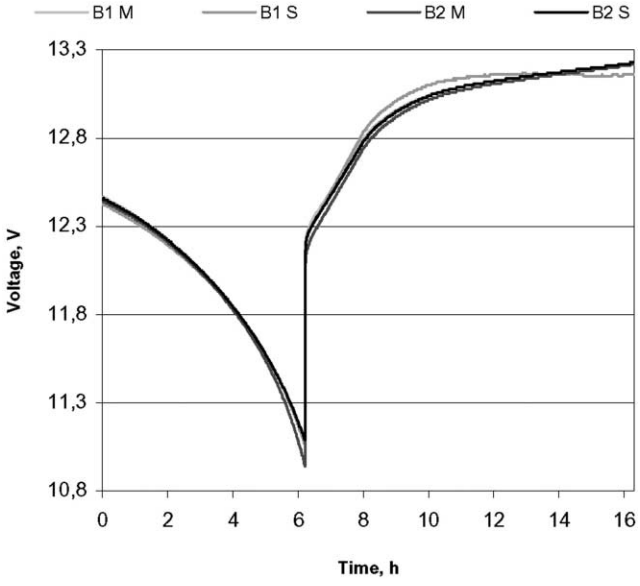

Fig. 4. Comparison of measured (M) and simulated (S) voltage for test batteries: B1–B2 of type A.

buried under insulating lead sulphate is not reachable for electron transfer because of low conductivity. This material is passive in electrochemical system, and is not shown in Tables 7 and 8. Total mass of passive and active material can be partially evaluated on the basis of model (3) for deposition coverage. About 10% more material can be evaluated using this model.

The battery capacity evaluated by model is different for every battery (Fig. 5). The active mass and battery capacity are strongly related. For example, battery number 2 is the weakest by charge and by total mass of active material in batteries of type A. The battery number 1 is the weakest by both parameters in batteries of type B.

Thickness of electrodes and separator and morphology of electrodes is different for every battery. Similarly, the charging–discharging curves in Fig. 4 (compare the end part of discharge curve) and the backup times and cut-off times in Tables 9 and 10, respectively, are different.

Thickness of electrodes and separator and morphology of electrodes can change during lifetime cycling of battery. Initial differences between manufactured batteries can be tested and the changes during lifetime observed.

Table 6
Average and maximum least square error of model

Model error (mV)	Battery 1	Battery 2	Battery 3	Battery 4
Average	0.02	0.04	0.03	0.02
	0.08	0.08	0.07	0.07
Maximum	37	51	52	42
	48	112	90	75

Table 7
Active mass and electrolyte volume of test batteries of type A

	Positive electrode (kg)	Electrolyte (dm^3)	Negative electrode (kg)	Total (kg)
Battery 1	1.794	0.831	1.431	4.288
Battery 2	1.526	0.775	1.230	3.748
Battery 3	1.687	0.821	1.370	4.107
Battery 4	1.646	0.813	1.364	4.051

Table 8
Active mass and electrolyte volume of test batteries of type B

	Positive electrode	Electrolyte	Negative electrode	Total
Battery 1	1.555	0.730	0.963	3.453
Battery 2	2.110	0.806	1.357	4.500
Battery 3	2.124	0.817	1.367	4.537
Battery 4	2.103	0.795	1.354	4.475

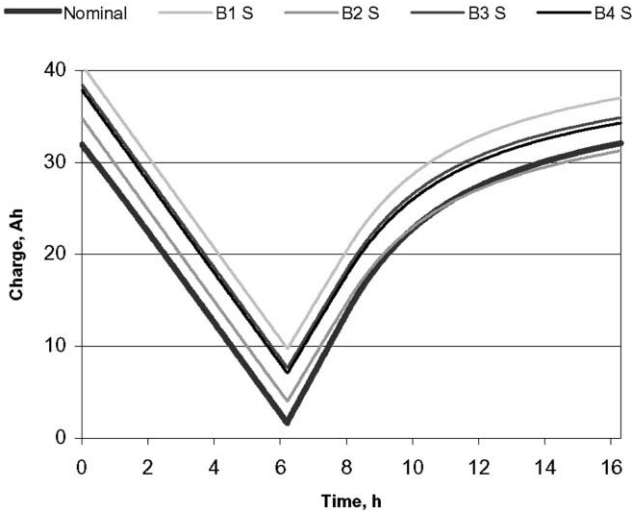

Fig. 5. Comparison of nominal and simulated (S) voltage for test batteries B1–B4 of type A.

Table 9
Backup time (min) for test batteries 1–4 in dependence on load

	Load (A)				
	5	10	20	35	50
Battery 1	404	202	100	57	40
Battery 2	365	182	91	52	36
Battery 3	400	200	99	57	39
Battery 4	398	199	99	56	39

Table 10
Cut-off time (min) for test batteries 1–4 in dependence on load

	Load (A)				
	5	10	20	35	50
Battery 1	455	226	111	60	38
Battery 2	412	206	103	57	37
Battery 3	451	224	110	59	38
Battery 4	448	222	110	59	38

The thickness of electrodes and separator and morphology of electrodes can be quickly evaluated from current–voltage measurements using proposed calculation model (Section 3) and automatic calibration algorithm.

7. State estimation

The electrochemical processes in battery can be evaluated online by current–voltage measurements. They are shown in Figs. 6–12. Measured data (applied current, voltage and temperature in container) were used to evaluate unobservable processes by recorded data on test battery 1. A full cycle from fully charged battery to deep discharge and back to the state of fully charged battery is shown.

Electrolyte overpotential depends weakly on location and strongly on discharge time. It has highest (absolute) values in the end of discharge and at the beginning of charge.

The volumetric reaction rate depends weakly on location in electrode and strongly on discharge time. Reaction is well balanced if battery is normally charged. It is less stable in the end of discharge and at the beginning of charging process.

Because part of the current is transferred to solid matrix, current density in liquid phase depends on location in electrode as linear function; it is constant in separator.

Acid concentration depends weakly on location in electrode and strongly on discharge time. Because of diffusion, acid concentrations in positive electrode, negative electrode, and separator are nearly equal. There is no indication that acid depletion is limiting factor for the current applied in Fig. 8.

The stratification of acid was observed (Fig. 10) at much higher discharge current for $C/I = 1$ h. The acid concentration depends strongly on location in electrode. It is lower at

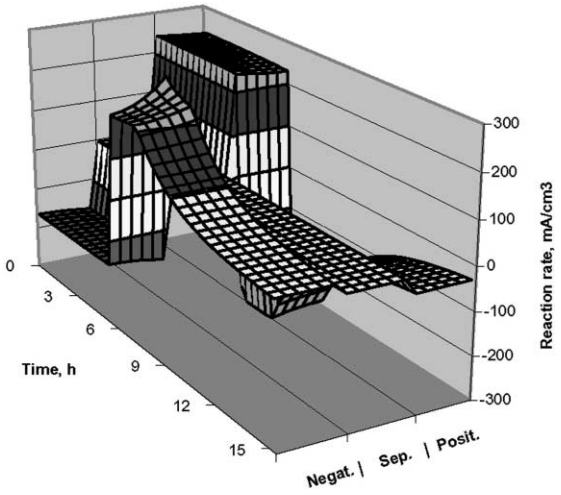

Fig. 7. Volumetric reaction rate.

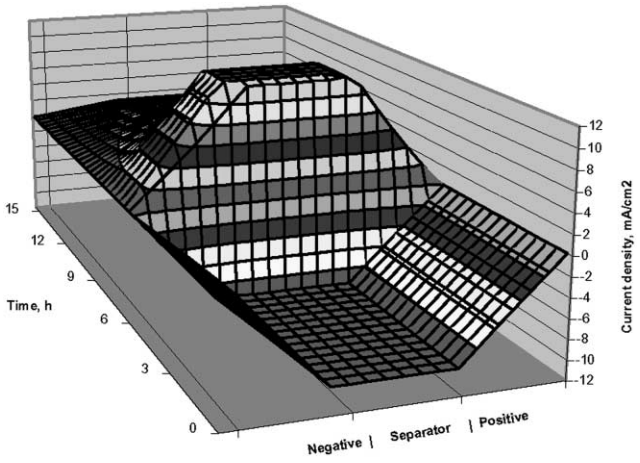

Fig. 8. Current density in electrode.

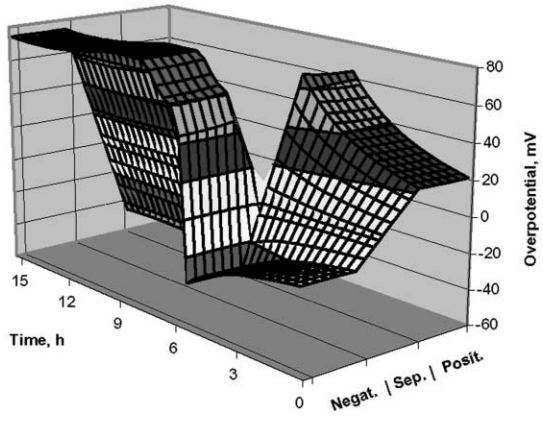

Fig. 6. Electrolyte overpotential (vs. hydrogen electrode).

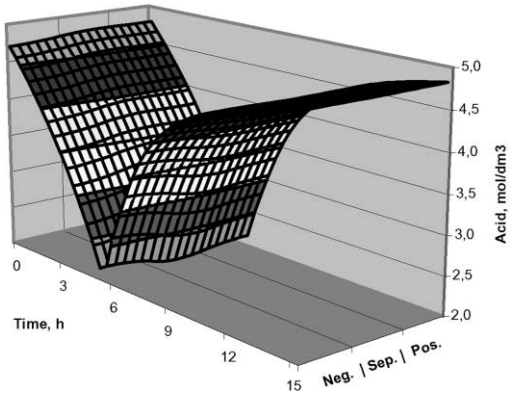

Fig. 9. Acid concentration in electrode (5 A).

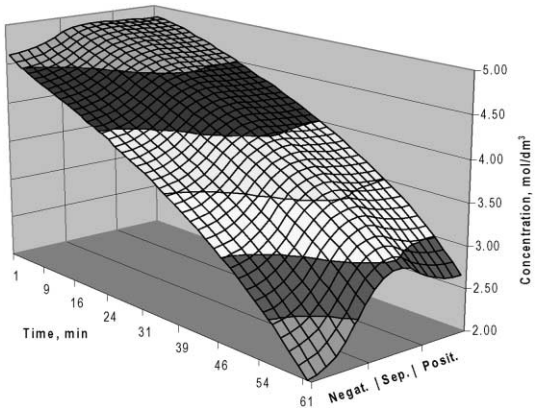

Fig. 10. Acid concentration in electrode (30 A).

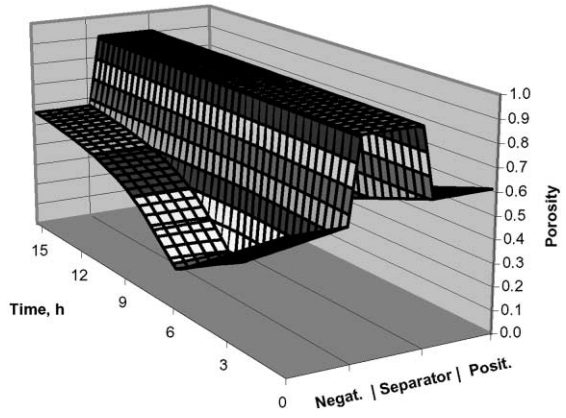

Fig. 11. Porosity of electrode.

positive electrode in comparison with negative electrode and especially in the end of discharge. The diffusion process of acid from separator is limited, it cannot equalise concentrations in positive and negative electrodes. However, even this applied current (30 A) was not high enough to show acid depletion which was observed when discharge current of over 50 A was used.

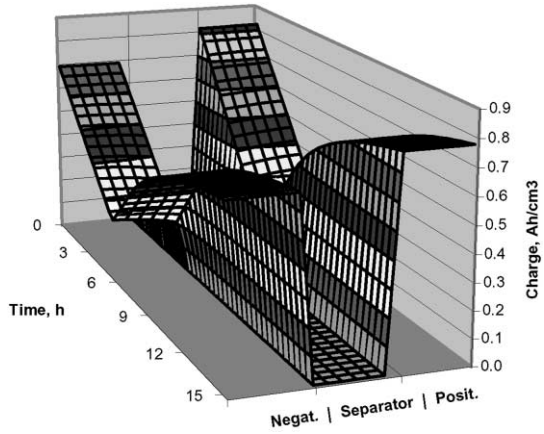

Fig. 12. Electrode capacity.

Porosity depends weakly on location in electrode and strongly on discharge time. It is lower in negative electrode in comparison with positive electrode and in the end of discharge. Porosity is highest in a fully charged battery.

Electrode-specific capacity depends weakly on location in electrode and strongly on discharge time. Electrode material discharge from fully charged to deep discharge and back to fully charge is shown in Fig. 12.

There is good evidence in Figs. 6–12 that a much faster lumped parameter model can be used for evaluation of the processes in battery if the discharging rate is relatively low. The observed electrochemical processes are nearly independent of their location in electrode. The discharging rate $C/I = 5$ h was used in the experiment. To some extent, higher discharging rates $C/I > 1$–2 h can be expected in a telecommunication UPS system. In this case, a distributed parameter model should be used. In most cases, batteries can be approximated with lumped parameter model or low-dimension model in monitoring of a telecommunications UPS system.

8. Evaluation of backup batteries

The battery model should be first calibrated and then used for analysis. In the following simulation, backup times and cut-off times of test batteries were evaluated.

The backup time is defined at level where 90% of battery capacity is used up. The cut-off time is defined at level where battery voltage drops below 9.3 V. This corresponds to cell voltage of 1.55 V/cell, a standard cut-off level for high-rate discharge used by battery manufacturers.

The backup time and cut-off time of the test batteries 1–4 of type A on discharge current of 5–50 A at temperature of 40°C is shown in Tables 9 and 10, respectively.

The effect of acid depletion can be seen at 50 A load. On higher loads, acid depletion becomes the limiting factor of fully utilising the battery capacity. The backup time for cold cracking (low temperature test) can be evaluated in the same way.

It can be seen from the results that battery 2 is weaker than others. Actually, its capacity is 35 Ah at 42°C against other batteries 41 Ah (battery 1), 39 Ah (battery 3), and 38 Ah (battery 4). The nominal capacity of these batteries is 30 Ah.

Telecommunications UPS system is designed for nominal battery capacity and load with some reserve. Real backup time being lower than nominal is considered as a battery failure.

9. Implementation

Real-time simulation software was developed for calculation of unobservable processes by observable processes (state estimation algorithm), model calculation (simulation algorithm) and model calibration (identification algorithm). Single battery or up to 10 batteries in string can be analysed with this software. It is designed to be integrated in a

telecommunications UPS system as a prototype for battery monitoring software.

10. Conclusion

It is shown in this paper that theoretical cell model can be calibrated to match rather accurately with measured data. This allows model-based evaluation of unobservable electrochemical processes in battery. Battery monitoring can be rendered fully automatic. Backup time and cut-off time — important parameters for telecommunications UPS system — can be tested quite easily. However, battery model should be calibrated periodically for every battery (case sensitive approach).

More information on state-of-health of battery can be withdrawn from applied model and direct current–voltage measurements than from conductivity or impedance measurements.

The electrochemical processes are in weak dependence of location in electrode at lower discharge rates. A common loading range $C/I < 2$–5 h for telecommunications UPS system allows using a really fast (10^5+ times faster than physical process) lumped parameter model or low-dimension model for system monitoring.

The model accuracy is limited due to some ignored processes. The following two improvements are important for monitoring of batteries in a UPS system:

1. More accurate models should be developed to predict gas formation processes for battery in overcharging conditions.
2. Dynamics of the double-layer should be accounted for in the calculation model. As a result, battery switched from charge to discharge frequently can be evaluated more precisely.

References

[1] F. Huet, A review of impedance measurements for determination of the state-of-charge or state-of-health of secondary batteries, J. Power Sources 70 (1998) 59–69.
[2] J. Newman, W.H. Tiedemann, AIChE J. Control Optim. 21 (25) (1975).
[3] W.H. Tiedemann, J. Newman, in: S. Gross (Ed.), Battery Design and Optimisation, The Electrochemical Society Softbound Proceeding Series, Princeton, New York, 1979, 23 pp.
[4] H. Gu, T.V. Nguyen, R.E. White, A mathematical model of a lead acid cell: discharge, rest and charge, J. Electrochem. Soc. 134 (12) (1987) 2953–2960.
[5] T.V. Nguyen, R.E. White, H. Gu, The effects of separator design on the discharge performance of a starved lead acid cell, J. Electrochem. Soc. 137 (10) (1990) 2998–3004.
[6] E.C. Dimpault-Darcy, T.V. Nguyen, R.E. White, A two-dimensional mathematical model of a porous lead dioxide electrode in a lead acid cell, J. Electrochem. Soc. 135 (2) (1988) 278–285.
[7] D.M. Bernardi, H. Gu, Two-dimensional mathematical model of a lead acid cell, J. Electrochem. Soc. 140 (8) (1993) 2250–2258.
[8] H. Gu, C.Y. Wang, B.Y. Liaw, Numerical modelling of coupled electrochemical and transport processes in lead acid cell, J. Electrochem. Soc. 144 (6) (1997) 2053–2061.
[9] D. Simonsson, P. Ekdunge, M. Lindgren, Kinetics of the porous lead electrode in the lead acid cell, J. Electrochem. Soc. 135 (7) (1988) 1614–1618.
[10] P. Ekdunge, D. Simonsson, The discharge behaviour of the porous lead electrode in lead acid battery. I. Experimental investigation, J. Appl. Electrochem. 19 (1989) 127–135.
[11] J. Landfors, D. Simonsson, A. Sokirko, Mathematical modelling of a lead acid cell with immobilised electrolyte, J. Power Sources 55 (1995) 217–230.
[12] D. Berndt, R. Bräutigam, U. Teutsch, Temperature compensation of float voltage, the special situation of VRLA batteries, in: Proceedings of the 7th International Telecommunications Energy Conference, The Netherlands, 1995, pp. 1–12.
[13] D. Berndt, Maintenance-Free Batteries, Research Studies Press Ltd./ Wiley, New York, 496 pp.
[14] D.M. Bernardi, M.K. Carpenter, A mathematical model of the oxygen-recombination lead acid cell, J. Electrochem. Soc. 142 (8) (1995) 2631–2642.
[15] H. Huang, T.V. Nguyen, A two-dimensional transient thermal model for valve regulated lead acid batteries under overcharge, J. Electrochem. Soc. 144 (6) (1997) 2062–2068.
[16] J. Newman, W. Tiedemann, Simulation of recombination lead acid batteries, J. Electrochem. Soc. 144 (9) (1997) 3081–3091.
[17] P. Ekdunge, D. Simonsson, The discharge behaviour of the porous lead electrode in lead acid battery. II. Mathematical model, J. Appl. Electrochem. 19 (1989) 136–141.
[18] S. Pissanetzky, Sparse Matrix Technology, Academic Press, New York, 1984.
[19] M.P. Vinod, K. Vijayamohanan, Effect of gelling on the open circuit potential against time transients of $Pb/PbSO_4$ electrodes at various state of charge, J. Appl. Electrochem. 24 (1994) 44–51.